Supporting Information

The Ultrafast Assembly of a Dipeptide Supramolecular Organogel and its Phase Transition from Gel to Crystal

Tingting Yuan,Dr. Youqian Xu,Dr. Jinbo Fei,HuiminXue, Xianbao Li, Chenlei Wang, Prof.Dr. George Fytas,Prof.Dr. Junbai Li

Ultrafast Assembly of Dipeptide Supramolecular Organogels and Phase Transition from Gel to Crystal

Tingting Yuan,[a, b] Jinbo Fei,[a] Youqian Xu,[a, b] Huimin Xue,[a, b] Xianbao Li,[a, b] Chenlei Wang,[a, b] George Fytas,[*, c] and Junbai Li[*, a, b]

Abstract: We report that gel-to-crystal phase transition of a dipeptide supramolecular assembly mediates active water transportation in oils. Addition of water into ultrafast assembled dipeptide organogels can induce a lamellar-to-hexagonal structural transformation of dipeptide molecular arrangement. Consequently, a phase transition from gel to crystal occurs and in turn water transports in the dipeptide crystal with well-defined channels. At macroscopic scale, water transport in the bulk system exhibits an anisotropic characteristic, which can be tuned by the presence of ions with the Hofmeister series. These favourable features enable automatic separation of dispersed nanoparticles from dissolved electrolytes in aqueous solution. Our findings demonstrate the potential of such assembled system for active filtration without external pressure.

Supramolecular assembly based on non-covalent interactions is a powerful strategy to construct well-ordered functional architectures.[1] Such assembled systems show great promise in a wide range of applications, such as optoelectronics, catalysis, biomedicine, chemical separation and artificial photosynthesis.[2] Owing to their dynamic and adaptive nature, the structure and function of supramolecular assemblies are tunable by small variations of the molecular arrangements.[3] In particular, controlled assembly of a single component facilitates permits formation of multiple phases with rich diversity of physical and chemical properties.[4] In view of this point, we envision that phase transition of supramolecular assembly can permit unique functions and applications.

Diphenylalanine (FF), as the core recognition motif of Alzheimer's β-amyloid polypeptide, has attracted increasing attention due to its excellent assembly, simple structure and ease of chemical derivatization.[5] As the pioneering group, Gazit and his coworkers have extended the applications of FF-based assemblies from semiconducting into biomedicine and nanofabrication.[6] Ulijn's group has developed various hydrogels based on FF derivatives toward novel bioapplications.[7] In our previous reports, a plethora of FF-based structures have been fabricated in a controlled manner towards optical waveguiding.[8] It is worth noting that as a low-molecular-weight gelator, FF readily self-assembles to form supramolecular organogels in pure or mixed oils.[9] In addition, responsive gel-to-crystal and gel-to-sol phase transitions can be triggered by various external and internal stimuli, such as light, pH, temperature, ionic strength and the choice of solvents.[10]

[a] T. Yuan, Dr. J. Fei, Dr. Y. Xu, H. Xue, X. Li, C. Wang, Prof. Dr. J. Li.
Beijing National Laboratory for Molecular Sciences (BNLMS), CAS Key Lab of Colloid, Interface and Chemical Thermodynamics, Institute of Chemistry, Chinese Academy of Sciences
Beijing 100190, China.
E-mail: jbli@iccas.ac.cn
T. Yuan, J. Fei and Y. Xu contributed equally to this work.
[b] T. Yuan, Dr. Y. Xu, H. Xue, X. Li, C. Wang, Prof. Dr. J. Li.
University of Chinese Academy of Sciences, Beijing 100049, China.
[c] Prof. Dr. G. Fytas
Max Planck Institute for Polymer Research, Ackermannweg 10, 55128 Mainz, Germany
E-mail: fytas@mpip-mainz.mpg.de
Supporting information for this article is given via a link at the end of the document.

Water has very limited solubility in oils like benzene, toluene and trichloromethane.[11] The high surface tension makes water transportation in such media difficult[12] and phase separations will usually occur. Traditionally, surfactants were introduced to generate water-in-oil, oil-in-water or more complex emulsions.[13] Recently, many reports focus on ways to achieve directional water transportation along a solid surface by constructing well-defined architectures and/or performing chemical modifications.[14] Nevertheless, active movement of water in immiscible oils seems not to have been reported, so far.

In this communication, we introduce a dipeptide supramolecular assembly-mediated active water transport in oils. As shown in Figure 1, dipeptide supramolecular assembly can form networks in hydrophobic organic solvents, accompanying molecular conformation and structural transformation. When water is added, a transition of the dipeptide organogel to hexagonal nanocrystal is induced, which in turn leads to further water transport. Such a transport behavior shows active and anisotropic characteristics. In particular, ions in aqueous solution show the typical Hofmeister effect on the speed of water transport. Interestingly, water migrates across the dipeptide supramolecular network, while nanoparticles larger than 1 nm remain at the initial water/oil interface. This finding points at potential applications for active solid-liquid microphase separations.

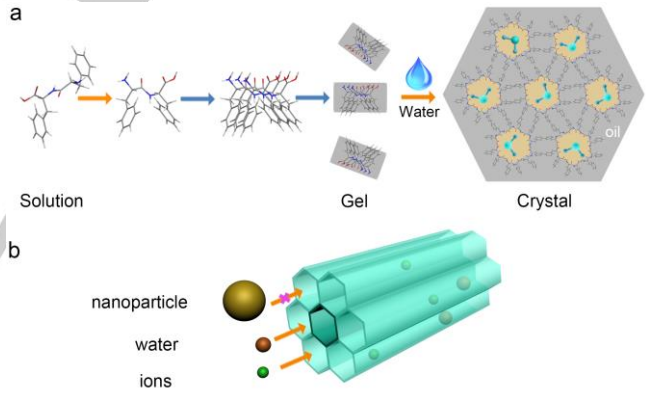

Figure 1. (a) Schematic illustration of phase evolution in dipeptide-based systems along probable molecular conformation (unfolding to folding) and arrangement changes (lamellar to hexagonal) in the dipeptide solution, gel and crystal. (b) Selective separation of nanoparticle from water and ions in solution after phase transition of dipeptide supramolecular assembly.

Dynamic light scattering (DLS) was utilized to investigate the structure of FF in solution, pre-gel and gel, respectively. FF was completely dissolved in 1,1,1,3,3,3-hexafluoro-2-propanol (HFIP) to form FF/HFIP solutions. Figure 2 depicts the relaxation function, C(q, t), for three FF concentrations (0.0025, 0.005, and 0.1 g/mL) at a scattering wave vector q=0.0201 nm^{-1} and 293 K. C(q, t) probes the diffusion of the scattering moieties over a submicrometer length (~2π/q). The bimodal C(q, t) could be represented (solid lines) by a double-exponential decay measuring the diffusion $D_i=\Gamma_i/q^2$, where the decay rate Γ_i refers to the fast (f) or the slow (s) rates. The slow process relates to relatively large species present in minor amount since their contribution to the amplitude of C(q, t) scales with their volume. The fast diffusion D_f and the associated scattering c/I_f intensity are concentration (c) dependent, as shown in the inset to Figure 2a. The size of the fast diffusing species is reflected by the

hydrodynamic radius, $R_h=k_BT/6\pi\eta_0D_f(0)$, where k_B, T, η_0 and $D_f(0)$ are the Boltzmann constant, temperature, solvent viscosity and diffusion at zero FF concentration, respectively. The latter is obtained from the linear dependence $D_f=D_f(0)[1+k_dc]$ with $k_d=2A_2M-(k_f+v)$ given by the friction coefficient k_f, the specific solute volume v, the molar mass M, and the second virial coefficient A_2. A_2 is positive and large (~0.1 $cm^3\ g^{-2}$ mol) in HFIP as revealed by the linear dependence of the expression $c/I_f = 1/M(1+2A_2c)$ shown in the inset to Figure 2a. The hydrodynamic radius, R_h=0.8 nm, compares favorably with the size of FF in a trans conformation. The friction, k_f+v ~ 66 cm^3/g, of the FF molecules in HFIP is substantially high.

The good solubility of FF in HFIP (high and positive A_2) is keeping even at a high FF concentration (0.1 g/mL) in solution (Figure 2a). However, when toluene was added into FF/HFIP solution, the system was at the solution state for FF concentrations was up to 0.00045 g/mL (Figure 2b). The relaxation function C(q, t) of FF in the HFIP/toluene (volume ratio 1:25) at q=0.0077 nm^{-1} relaxes, at long times, to zero for FF concentrations lower than 0.00045 g/L. The full relaxation, implies an equilibrium (ergodic) behavior. A similar analysis of the C(q, t) unexpectedly reveals a significantly faster diffusion (1.36×10^{-5} cm^2/s) in FF/ HFIP/toluene appears, compared with that (1.50×10^{-6} cm^2/s) in FF/HFIP (the insets, Figure 2a and 2b). Taken into account the different solvent viscosities, this disparity could be only by factor of 3. The friction coefficient k_f decreases remarkably from 66 to ~0 cm^3/g meaning that the toluene/HFIP (25:1) binary mixture acts as a theta solvent ($A_2\approx0$, inset to Figure 2b). It is conceivable that in the binary solvent, co-solvency can have a profound effect on the structure of FF.

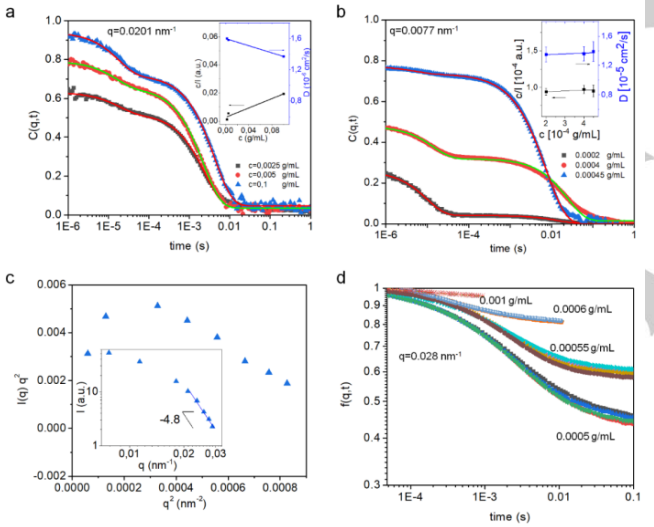

Figure 2. (a) Relaxation functions C(q,t) for the translation diffusion of FF in HFIP at three concentrations (c), (square, 0.0025 g/mL; circle, 0.005 g/mL; triangle, 0.1 g/mL) at a scattering wave vector , q=0.0201 nm^{-1}) and 293 K. The solid lines indicate the representation of C(q,t) by double-exponential decay. The reduced scattering intensity c/I and diffusion coefficient D as a function of FF concentration are shown in the inset. (b) Relaxation functions C(q,t) for the translation diffusion of FF for three concentrations (square, 0.0002 g/mL; circle, 0.0004 g/mL; triangle, 0.00045 g/mL) in HFIP/toluene (1:25 v/v) at q=0.0077 nm^{-1}) and 293 K. The solid lines indicate the representation of C(q,t) by double-exponential decay. The reduced c/I and diffusion coefficient D as a function of FF concentration are shown in the inset. (c) The intensity pattern, $I(q)*q^2$ vs. q^2 at 0.00045 g/mL along with the double logarithmic presentation of I(g) vs q in the inset. The intensity drops strongly with q ($I(q) \propto q^{-4.8}$) at high q. (d) The normalized dynamic structure factor for four concentrations in the weak gel regime recorded at θ=140° and 293 K for different positions. The plateau of f(q,t) at decay times denotes increased fraction of the frozen-in inhomogeneity with FF concentration.

Turning to the slow process of C(q, t), its contribution becomes significant at 0.00045 g/mL, a very low FF concentration compared with FF in HFIP (Figure 2a). The associated large species have still a dimension comparable to q^{-1}, hence the Holtzer presentation, $q^2I_s(q)$, of the scattering intensity $I_s(q)$ in Figure 2c displays the characteristic peak at q*~π/R with R being the overall size of the slow supramolecular FF assembly. However, $q^2I_s(q)$ should become q-independent at high q's if the structure is a thin coil. Instead, in the double logarithmic I(q) vs. q presentation in the inset to Figure 2c reveals strong drop in $I(q) \propto q^{-4.8}$ at short length scales reminiscent of solid cross-section of this supramolecular assembly (Porod law) associated with the slow process (Figure 2b). Thus, a network is formed through the overlapping of the worm-like chains with large cross-sectional radii. The relaxation function C(q,t) becomes position dependent, characteristic of a non-ergodic behavior and already at c=0.0005 g/mL the normalized correlation function f(q,t) does not decay to zero within the longest time of the experiment. This non-zero baseline f(q,∞), which is a measure of the frozen-in concentration fluctuations in the weak gel state, increases rapidly with the FF concentration (Figure 2d). f(q,t) is computed from the experimental intensity correlation function G(q,t), which is recorded at different sample positions (Figure S1). The dynamic fraction of the concentration fluctuations is characterized by a fast diffusion coefficient increasing rapidly from 7.5×10^{-9} to 5.2×10^{-8} cm^2/s for 0.0005 to 0.0006 g/mL, respectively. This indicates cooperative diffusion or fast diffusion that speeds up with concentration due to the strong decrease of the network mesh size.

Taken together, the hydrodynamic radius R_h of FF as a function of FF concentration in HFIP and toluene/HFIP, are shown in Figure S2a and 2b, respectively. It might suggest a folded structure of FF as indicated by the very low R_h~0.3 nm (black squares and scheme in Figure S2b). We recall, that R_h=0.8 nm in HFIP (scheme in Figure S2a). This dramatic drop of the FF size occurs upon addition of toluene in HFIP even at 10% (toluene/HFIP ratio 1:9) (Figure S2b, S3 and S4). Hence, the behavior of FF in toluene/HFIP pre-gel state is very different from that in neat HFIP solution. In addition, the cooperative diffusion of the systems depends strongly on the FF concentration, indicating a formation of a three-dimensional network (Figure S2c). At 0.001 g/mL the solution turns predominantly non-ergodic as it enters the organogel regime.

Interestingly, it is found that transparent FF supramolecular organogel forms in the above solvents within 3 seconds when the concentration of the gelator is above 0.005 g/mL. Upon addition of water, such assembled organogel gradually became opaque from top to bottom, as shown in Figure 3a. This appearance indicates modified dipeptide supramolecular assembly. Figure 3b reveals that the morphology of molecular assembly changes from ultrafine fiber to wider and longer nanofibers. For comparison, when the same amount of chloroform was introduced into the gel, there was no obvious change in the system besides an increase in volume (Figure S5). Fourier transform infrared spectroscopy (FTIR) was implemented to investigate the effect of molecular interactions before and after the morphology transformation. Figure 3c shows the xerogel has a strong absorption peak at 1681 cm^{-1}, which is the characteristic peak of N–H stretching vibration in amide I band, and an absorption peak at 1602 cm^{-1}, which belongs to amide II absorption band. The same adsorption was also detected in the organogels treated by water. It indicates that β-sheet secondary structure with antiparallel alignment exists even after water treatment. Obviously, the absorption peak at 1602 cm^{-1} becomes clearer after completion of the morphology transformation. This appearance may be resulted from the

impact of the water treatment on the interaction of C=O and N–H moieties in the FF assembly.[15]

X-ray diffraction (XRD) was used to demonstrate the phase transition induced by water. According to Figure 3d and S6, the peaks at 5.12° and 10.03°, corresponding to 1.72 and 0.88 nm spacing, respectively are virtually concentration independent over the range at which the organogel transforms from a viscous liquid to a solid gel. The spacing ratio of 1: 0.5 is consistent with a lamellar structure.[16] This spacing represents the interlamellar distance generated by FF molecules in the same fiber. After water treatment, as shown in Figure 3d, sharp peaks appear, which is strong evidence for the formation of a hexagonal structure.[17] In the formation process of the organogel, the aromatic ring of toluene is involved in π-π stacking interactions with FF molecules. After addition of water, the original lamellar β-sheet structure curls and rearranges into the more stable hexagonal structure. Circular dichroism (CD) spectroscopy was employed to investigate the changes of the secondary structures in the FF supramolecular assembly before and after the phase transition. As shown in Figure 3e, FF organogel did not display obvious CD signals, indicating the absence of chirality in the gel phase. As a comparison, in the crystalline phase, FF assembly exhibits a single negative band with a peak at 278 nm, conforming to its intrinsic molecular configuration.[18] The CD results suggest that a phase transition from an FF gel to a crystalline state is associated to chirality of FF supramolecular assembly.

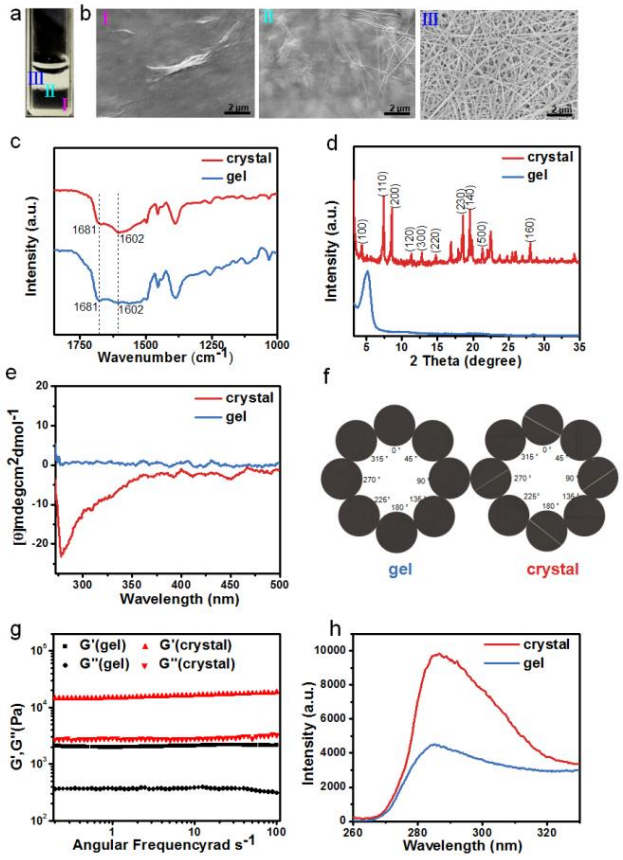

Figure 3. (a) Optical image of two phases in FF organogel after introducing water from the top (the concentration of FF is 0.005 g/mL). (b) Corresponding SEM images. (I) FF organogel; (II) phase boundary; (III) FF crystalline. (c) FTIR spectra, (d) XRD patterns, (e) CD spectra, (f) Cross-polarized microscopy images, (g)dynamic storage (G'') and loss (G'') moduli at 293K and (h) photoluminescence emission spectra (upon excitation at λ= 250 nm) of the organogel(0.005 g/mL) before and after water treatment.

The refractivity from the gel and crystal phases was investigated by a cross-polarized microscope. As shown in Figure 3f (right panel), the maximum birefringence was recorded in the crystalline phase when the fibers are aligned normal to the polarizer. For 45° fiber orientation to the polarizer the recorded birefringence became very weak. In contrast, there were no such effects in the optically isotropic gel phase (Figure 3f, left panel). Hence, the water-induced phase transition of FF supramolecular network generates anisotropic fibers. The structural changes were also manifested in the shear rheometry of the supramolecular assembly. The dynamic shear modulus (G') and loss modulus (G'') before and after phase transition are shown in Figure 3g. In the frequency range 0.15-100 rad s^{-1} (at a constant strain of 0.1%), in gel and crystal phases, both the G' and G'' values depend slightly on the probed frequency and G' is always larger than G''. The mechanical strength of the system increased sharply by a factor of ten upon completion of the transition from an FF gel to a crystalline state. In addition, the maximum intensity of the fluorescence spectrum of the system after the phase transition increased by more than a factor of two compared to the spectrum of the gel (shown in Figure 3h). It may be caused by the reduced vibration and rotation of the excited state molecules in the crystal state.

To investigate the water transport, the organogel containing 0.005 g/mL FF was selected in view of its robustness. When the same amount of water is added into the gel from top, middle and bottom, the covered distance and speed are distinct. In detail, when a water drop (1.5 μL) were injected on the top of the gel (Figure S7a, top and S7b), the water droplets had a spreading phenomenon at a rate of 0.60 cm/h in the horizontal direction, so the phase along this direction transition completed within in one hour. As for the vertical direction, the speed was much slower (0.10 cm/h). When water drops were injected into the middle, the gel started to form fibers surrounding the drop about one hour later (Figure S7a, middle and S7c), before water transported through the system. When a water drop with a volume of 1.5 μL was injected into the gel, the phase transition region appeared ellipse-like. At 6 h later, the full volume of gel became slightly opaque, while a larger ellipse-like region was still present in the middle of the gel. After 8 h, the gel became white. The speeds in the horizontal direction and vertical direction were respectively, 0.067and 0.042 cm/h, suggesting an anisotropic water mobility in the supramolecular gel is anisotropic.

Furthermore, in our system, water transport can overcome the gravity effect. To verify this point, a water drop of 1.5 μL was injected at the bottom of the gel (Figure S7a, bottom and Figure S7d), thereby inverting the flow direction. The speeds in horizontal and vertical direction were 0.100 and 0.073 cm/h, respectively, again corroborating the notion of an anisotropic flow through the FF-assembled fiber. However, because of the gravity effect the flow was much slower than in the opposite top to bottom direction (0.10 cm/h). Taken together, as a comprehensive comparison, Figure S7e shows that in the horizontal direction, when a water drop is added in the middle, the transporting distance is slightly shorter than when the water drop is added at the bottom. As for the vertical direction, at the same time, when the drop is introduced from the top of the gel, the water covered distance is longer than when water is added from the middle or the bottom. This could be explained by the gravity effect.

The amount of water added was found to be an important factor affecting the transfer behavior. As shown in Figure S8, the extent of the transformed regions gradually increased in parallel with the amount of water droplets (0.5, 1 and 2 μL) injected at the bottom of the gel. Quantitatively, as revealed in Figure S8b and S8c, the water transport rates during the first four hours for both horizontal and vertical directions were 0.08 and 0.05 cm/h

for 0.5 µL, 0.10 and 0.07 cm/h for 1 µL, 0.11 cm/h and 0.10 cm/h for 2 µL, respectively. (Since the radius in the horizontal direction is 0.6 cm, the phase transition of the samples with water drops of 1 and 2 µL were completed in 5 h. Therefore, the transport rates increase with the increasing amount of water over the mentioned range. As revealed in Figure S9, water addition of more than 100 µL, results in the damage of gel structure. Further, water diffuses in random rather than directional manner. The phase transition completes within 2 h.

To investigate ionic effect on water transport, solutions containing typical cations or anions were added to the gel. As shown in Figure 4a, different transport rates were obtained for $Ca(NO_3)_2$ and $CaCl_2$. The phase transition was complete after 7 h for the $Ca(NO_3)_2$ solution, while for the $CaCl_2$ solution, only 57% of the organogel had turned into crystals over the same period of time. Similarly, the time for complete phase transition for KNO_3 and KCl aqueous solutions was 4 and 5.5 h, respectively, whereas the time was extended to 6 h for a KBr solution. The distinct transport rates for these electrolytes are probably associated to the hydrophobic effect, of the ions in accordance with the Hofmeister theory.[19] When the anion was Cl^- and the cations were either K^+, Na^+ or Ca^{2+} respectively, the plots in Figure S10 show that cations also influenced the speed of the water transport. For K^+ and Na^+ was approximately the same speed recorded, while a slower rate was registered for Ca^{2+}. Figure 4b summarizes for KCl, KNO_3, KBr, NaCl, $Ca(NO_3)_2$ and $CaCl_2$ solutions the time to induce gel phase transformation, respectively.

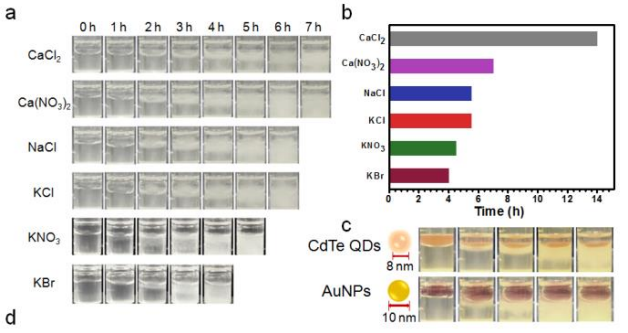

d

Item	Ca^{2+}	K^+	Na^+	Cl^-	NO_3^-	Br^-	CdTe QDs	AuNPs
Hydrated radius (Å)	4.12	3.31	3.58	3.32	3.35	3.30	~80	~100

Figure 4. (a) Optical images of the phase transition process of FF-toluene organogels after addition of different salt solutions. (b) Corresponding total times required to complete the phase transition. (c) Phase transition induced solvent transportation into the FF-toluene organogel for solid-liquid separation of CdTe QDs and AuNPs. (d) Hydrated radii of anions, cations and nanoparticles.

The ion permittivity experiments imply the presence of channels in the supramolecular assemblies. To estimate the channel pore, aqueous solutions containing Au nanoparticles (AuNPs) and CdTe quantum dots (CdTe QDs) were dropped softly on the top of the organogel. The dispersed nanoparticles did not penetrate the gel and remained on the top of the organogel (Figure 4c). After the water reached the bottom of the gel, the formed fibers were collected and measured by energy dispersive X-ray spectroscopy (EDX) to quantify the key elements. In the case of AuNPs, only the element Cl was detected in the gel, shown in Figure S11. Thus, AuNPs were separated from the solution. Following the same procedure, CdTe QDs were also excluded from the organogels. On the contrary, ions such as Ca^{2+}, K^+, Na^+, Cl^-, NO_3^- and Br^-, whose hydrated radii are less than 10 Å (Figure 4d),[20] can be detected by EDX (Figure S12). Hence these ions can go along with water transport from the top to the bottom. These penetration experiments indicate that the channels created via FF assembly is so narrow that only ions and small molecules can pass through. Based on the estimation of the mesh size $\xi \sim (kT/G')^{1/3}$ (24 nm at 0.005 g/mL), this cannot be related to the channel size. Instead, the FF assembly after phase transition exhibits a size exclusion effect, indicating that the gel can be used for separation of fine particles from dissolved ions.

As a perspective, similar phenomena can be found with other FF-based organogels. Figure S13a shows that in FF-$CHCl_3$/isoproponal(3%), FF-xylene and FF-CCl_4/DMF(2%) systems, after water was added into the gel, the phase transition from gel to crystal could be observed from top to bottom. This indicates that mediated by the assembled fibers, water can be transported through the hydrophobic organic solvent. The type of organic solvent affects the speed of the phase transition. The time needed with the different organogels is given in Figure S13b.The effect might result from differences in molecular interactions between FF and organic solvents in the organogels.

In summary, we demonstrate active water transport through oil mediated by a phase transition of ultrafast assembled dipeptide supramolecular organogels. Water readily triggers a gel-to-crystal phase transition of the dipeptide-based system, leading to formation of hexagonal nanocrystals with well-defined channels. In turn, water transports through the channels and induces further phase transition. Quantitatively, without any external pressure, the velocity of water transport in oil is around 0.10 cm/h. Moreover, the behavior of water transport in bulk exhibits an anisotropic feature. Ionic effect plays a key role in the transport velocity in the organogel, in good accordance with the Hofmeister series. As a comparison, nanoparticles cannot penetrate the system after phase transition of supramolecular organogel due to a size exclusion effect. It means the gel can be utilized for automatic separation of nanoparticles from dissolved electrolytes such as ions. The short peptide-based supramolecular assembly system has a potential for selective and effective purification or concentration of trace nanoparticles or proteins.

Acknowledgements

The authors gratefully acknowledge the financial support for this research from the National Nature Science Foundation of China (No. 21433010, 21872150 and 21573248). G. F. acknowledges partial support from ERC Ad G SmartPhon (No. 694977). J. F. particularly thanks the Youth Innovation Promotion Association of CAS (No. 2016032) and Institute of Chemistry, CAS (No. Y6290512B1).

Keywords: supramolecular assembly • dynamic light scattering• dipeptide • phase transition • water transport

[1] a) K. Ariga, D. T. Leong, T. Mori, *Adv. Funct. Mater.* **2018**, *28*, 1702905; b) R. Freeman, M. Han, Z. Alvarez, J. A. Lewis, J. R. Wester, N. Stephanopoulos, M. T. McClendon, C. Lynsky, J. M. Godbe, H. Sangji, E. Luijten, S. I. Stupp, *Science* **2018**, *362*, 808-813; c) T. Aida, E. W. Meijer, S. I. Stupp, *Science* **2012**, *335*, 813-817; d) K. Ariga, H. Ito, J. P. Hill, H. Tsukube, *Chem. Soc. Rev.* **2012**, *41*, 5800-5835.

[2] a) X. Li, J. Fei, Y. Xu, D. Li, T. Yuan, G. Li, C. Wang, J. Li, *Angew.Chem. Int. Ed.* **2018**, *57*, 1903-1907; *Angew. Chem.* **2018**, *130*, 1921-1925; b) A. S. Weingarten, R. V. Kazantsev, L. C. Palmer, M. McClendon, A. R. Koltonow, A. P. Samuel, D. J. Kiebala, M. R. Wasielewski, S. I. Stupp, *Nat. Chem.* **2014**, *6*,

964-970; c) K. Sano, Y. Ishida, T. Aida, *Angew. Chem., Int. Ed.* **2018**, *57*, 2532-2543; d) P. Xing, Y. Zhao, *Adv. Mater.* **2016**, *28*, 7304-7339; e) L. Yue, S. Wang, D. Zhou, H. Zhang, B. Li, L. Wu, *Nat. Commun.* **2016**, 7, 10742; f) Y. Xu, J. Fei, G. Li, T. Yuan, X. Xu, C. Wang, J. Li, *Angew. Chem. Int. Ed.* **2018**, *57*, 6532-6535; *Angew. Chem.* **2018**, *130*, 6642-6645.

[3] C. D. Jones, J. W. Steed, *Chem. Soc. Rev.* **2016**, *45*, 6546-6596.

[4] a) M. T. Fenske, W. Meyer-Zaika, H. G. Korth, H. Vieker, A. Turchanin, C. Schmuck, *J. Am. Chem. Soc.* **2013**, *135*, 8342-8349; b) P. Y. Dankers, T. M. Hermans, T. W. Baughman, Y. Kamikawa, R. E. Kieltyka, M. M. Bastings, H. M. Janssen, N. A. Sommerdijk, A. Larsen, M. J. van Luyn, A. W. Bosman, E. R. Popa, G. Fytas, E. W. Meijer, *Adv. Mater.* **2012**, *24*, 2703-2709.

[5] a) P. Makam, E. Gazit, *Chem. Soc. Rev.* **2018**, *47*, 3406-3420; b) L. Adler-Abramovich, E. Gazit, *Chem. Soc. Rev.* **2014**, *43*, 6881-6893.

[6] a) K. Tao, P. Makam, R. Aizen, E. Gazit, *Science* **2017**, *358*; b) S. Brahmachari, Z. A. Arnon, A. Frydman-Marom, E. Gazit, L. Adler-Abramovich, *ACS Nano* **2017**, *11*, 5960-5969; c) Z. A. Arnon, A. Vitalis, A. Levin, T. C. Michaels, A. Caflisch, T. P. Knowles, L. Adler-Abramovich, E. Gazit, *Nat. Commun.* **2016**, *7*, 13190; d) A. Levin, T. O. Mason, L. Adler-Abramovich, A. K. Buell, G. Meisl, C. Galvagnion, Y. Bram, S. A. Stratford, C. M. Dobson, T. P. Knowles, E. Gazit, *Nat. Commun.* **2014**, *5*, 5219.

[7] a) J. K. Sahoo, C. G. Pappas, I. R. Sasselli, Y. M. Abul-Haija, R. V. Ulijn, *Angew. Chem. Int. Ed.* **2017**, *56*, 6828-6832; *Angew. Chem.* **2017**, *129*, 6932-6936; b) C. G. Pappas, I. R. Sasselli, R. V. Ulijn, *Angew. Chem. Int. Ed.* **2015**, *54*, 8119-8123; *Angew. Chem.* **2015**, *127*, 8237-824.

[8] a) B. Sun, Q. Li, H. Riegler, S. Eickelmann, L. Dai, Y. Yang, R. Perez-Garcia, Y. Jia, G. Chen, J. Fei, K. Holmberg, J. Li, *ACS Nano* **2017**, *11*, 10489-10494; b) Q. Li, H. Ma, A. Wang, Y. Jia, L. Dai, J. Li, *Adv. Opt. Mater.* **2015**, *3*, 194-198.

[9] X. Liu, J. Fei, P. Zhu, J. Li, *Chem. Asian J.* **2016**, *11*, 2700-2704.

[10] a) P. Xing, Y. Li, Y. Wang, P. Z. Li, H. Chen, S. Z. F. Phua, Y. Zhao, *Angew. Chem. Int. Ed.* **2018**, *57*, 7774-7779; *Angew. Chem.* **2018**, *130*, 7900-7905; b) Y. Lan, M. G. Corradini, R. G. Weiss, S. R. Raghavan, M. A. Rogers, *Chem. Soc. Rev.* **2015**, *44*, 6035-6058; c) X. Yu, L. Chen, M. Zhang, T. Yi, *Chem. Soc. Rev.* **2014**, *43*, 5346-5371.

[11] L. A. Estroff, A. D. Hamilton, *Chem. Rev.* **2004**, *104*, 1201-1218.

[12] S. Daniel, M. K. Chaudhury, J. C. Chen, *Science* **2001**, *291*, 633-636.

[13] P. G. De Gennes, C. Taupin, *J. Phys. Chem.* **1982**, *86*, 2294-2304.

[14] a) Y. Zhang, M. Cao, Y. Peng, X. Jin, D. Tian, K. Liu, L. Jiang, *Adv. Funct. Mater.* **2018**, *28*, 1704220; b) Y. Zhao, C. Yu, H. Lan, M. Cao, L. Jiang, *Adv. Funct. Mater.* **2017**, *27*, 1701466.

[15] J. Wang, K. Liu, L. Yan, A. Wang, S. Bai, X. Yan, *ACS Nano* **2016**, *10*, 2138-2143.

[16] K. Lv, L. Zhang, W. Lu, M. Liu, *ACS Appl. Mater. Inter.* **2014**, *6*, 18878-18884.

[17] N. Hendler, N. Sidelman, M. Reches, E. Gazit, Y. Rosenberg, S. Richter, *Adv. Mater.* **2007**, *19*, 1485-1488.

[18] X. Liu, J. Fei, A. Wang, W. Cui, P. Zhu, J. Li, *Angew. Chem. Int. Ed.* **2017**, *56*, 2660-2663; *Angew. Chem.* **2017**,*129*, 2704-2707.

[19] P. S. Cremer, A. H. Flood, B. C. Gibb, D. L. Mobley, *Nat. Chem.* **2017**, *10*, 8-16.

[20] E. R.Nightingale, *J. Phys. Chem. C* **1959**, *63*, 1381-1387.

COMMUNICATION

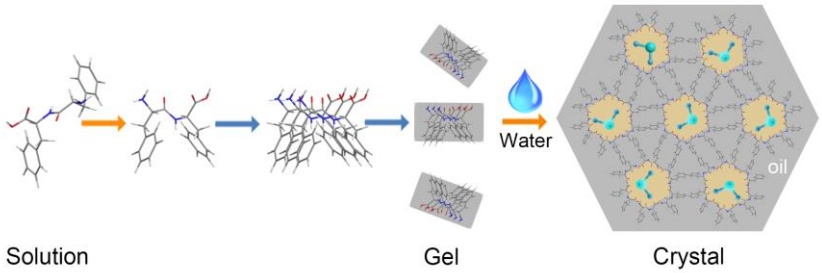

*Tingting Yuan, JinboFei, YouqianXu, HuiminXue, Xianbao Li, Chenlei Wang, George Fytas, * Junbai Li **

Page No. – Page No.
Ultrafast Assembly of Dipeptide Supramolecular Organogels and Phase Transition from Gel to Crystal

A gel-to-crystal phase transition of a dipeptide supramolecular assembly creates well-defined channels to direct water transportation through immiscible oils. Such assembled system holds a great potential for active purification or concentration of dispersed particles in aqueous solution.